Raman Spectroscopic Study on the Structure in the Surface and the Bulk Shell of $Ce_xPr_{1-x}O_{2-\delta}$ Mixed Oxides

Meng-Fei Luo,* Zong-Lan Yan, Ling-Yun Jin, and Mai He

Zhejiang Key Laboratory for Reactive Chemistry on Solid Surfaces, Institute of Physical Chemistry, Zhejiang Normal University, Jinhua 321004, China

Received: December 13, 2005; In Final Form: March 24, 2006

The difference between the surface and the bulk shell of $Ce_xPr_{1-x}O_{2-\delta}$ mixed oxides was studied by Raman spectroscopy with four different excitation lasers. Two Raman peaks appear at 465 and 570 cm^{-1} under all of the four lasers. The former is attributed to the Raman active F_{2g} mode of CeO_2, while the latter is attributed to oxygen vacancy. On the basis of the fact that the laser with shorter wavelength is closer to the electronic adsorption of samples, it is found that the Raman information detected by excitation laser with shorter wavelength is more sensitive to the surface region of samples. An inflection is observed in the relationship of the value I_{570}/I_{465} to the Ce content in $Ce_xPr_{1-x}O_{2-\delta}$. With the increase in the wavelength of excitation laser, the Ce content corresponding to the inflection decreases. Combined with the surface concentration obtained by XPS, it can be deduced that the composition of $Ce_xPr_{1-x}O_{2-\delta}$ mixed oxide particles in the surface region and the bulk shell are different, the former is enrichment of Pr component and the latter is enrichment of Ce component. The thickness of the surface layer with rich Pr component decreases with the increase in the Ce content.

1. Introduction

Cerium oxide is one of the most reactive rare earth metal oxides that has been extensively studied and employed in various applications, including catalysts, oxygen storage capacitors, ion conductors, UV blockers, and polishing materials.[1−5] Among these applications, the most relevant use of ceria is in catalysts, where it is used as a support or an active catalyst.[6] However, the thermostability of pure ceria under high-temperature conditions is poor, therefore its oxygen storage capacity (OSC) decreases greatly.[7,8] One approach to solving this problem is that the cerium ion in the ceria lattice is replaced by another ion so that a defective fluorite structure solid solution is formed such as Ce−Zr, Ce−La, Ce−Ti, Ce−Y, and Ce−Pr mixed oxides.[6,9−11] However, the previous investigations provided the information mainly on the bulk of ceria-based materials, and the structure in the surface region of ceria-based material particles has rarely been studied. For the mixed oxide materials, the composition of the surface region is always different from the bulk.[6] The surface property of the particle is very important for catalytic reactions and absorption capability because the catalytic reaction is produced mainly on the surface activity site of particles.

Raman spectroscopy is one of the most useful techniques for characterization of catalytic materials and catalytic reaction.[12−14] Recently, Li et al.[15,16] reported that UV Raman spectroscopy is a surface-sensitive technique for zirconia due to its strong absorption. Combined with the visible Raman spectra and XRD patterns, the UV Raman spectra indicate that the phase transformation in the surface region of zirconia particle is different from that in the bulk.

To get further insight into the difference in the structure between the surface and the bulk shell of ceria-based materials, as one of these, $Ce_xPr_{1-x}O_{2-\delta}$ mixed oxides are studied by using Raman spectroscopy with four excitation lasers, namely 325, 514, 633, and 785 nm.

2. Experimental Section

2.1. Preparation of Catalysts. A series of oxides with general formula $Ce_xPr_{1-x}O_{2-\delta}$ ($x = 0$, 0.2, 0.3, 0.5, 0.7, 0.8, 0.9, 0.95, 0.97, 0.99, 1.0) were prepared by a sol−gel method. For a $Ce_{0.8}Pr_{0.2}O_{2-\delta}$ sample, 0.08 mol of $Ce(NO_3)_3$ (99.9%) and 0.02 mol of $Pr(NO_3)_3$ (99.5%) were dissolved in 150 mL of H_2O, then 0.10 mol of citrate (99.5%) dissolved in 100 mL of H_2O was added to the above mixture solution. The mixture was then heated at 90 °C under stirring until it became transparent gel. The gel was further dried at 100 °C overnight and finally calcined at 900 °C for 4 h. Other samples with different Ce/Pr ratio were prepared in the same manner.

2.2. Characterization. Raman spectra were obtained by a Renishaw RM1000 confocal microscope. The exciting wavelengths are 325, 514, 632.8, and 785 nm with a power of ca. 3 mW on the sample. The resolution is ±1 cm^{-1}. To get the comparable data, the powder samples were pressed to form disks in a homemade mold. The scanning range was 200−1000 cm^{-1} in air. The experiments of in situ Raman spectra of the samples were performed using a home-built in situ Raman cell, which allows us to record the Raman spectra under different gas atmospheres such as air, O_2, and H_2. XPS measurements were performed on a Perkin-Elmer PHI 5000C spectrometer using Al Kα radiation (1486.6 eV) as the excitation source. Quantitative analysis of atomic ratios was accomplished by determining the elemental areas. UV−visible absorption spectra were recorded on a JASCO V-550 spectrophotometer equipped with an integrating sphere. X-ray diffraction (XRD) patterns were collected on a Philips PW3040/60 powder diffractometer operating at 40 kV/40 mA using Cu Kα radiation in the 2θ

* Corresponding author. E-mail: mengfeiluo@zjnu.cn. Fax: +86-579-2282595.

10.1021/jp057274z CCC: $33.50
Published on Web 06/14/2006

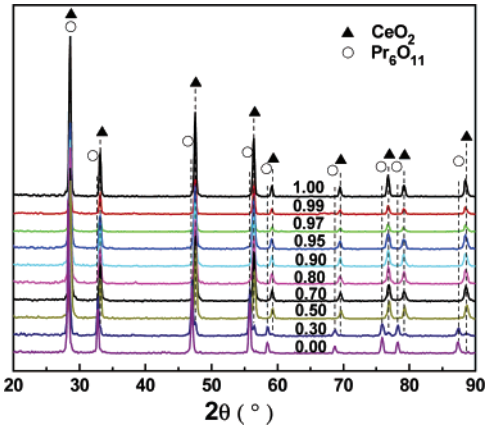

Figure 1. XRD patterns of $Ce_xPr_{1-x}O_{2-\delta}$ mixed oxides.

TABLE 1: Lattice Parameter and the Mean Crystallite Size of Cubic Phase for 111 Crystal Face ($2\theta = 28.5°$) in $Ce_xPr_{1-x}O_{2-\delta}$ Samples

samples	phase	lattice parameter (nm)	crystallite size (nm)
CeO_2	CeO_2	0.541	40.6
$Ce_{0.99}Pr_{0.01}O_{2-\delta}$	CeO_2	0.541	38.6
$Ce_{0.97}Pr_{0.03}O_{2-\delta}$	CeO_2	0.542	33.4
$Ce_{0.95}Pr_{0.05}O_{2-\delta}$	CeO_2	0.541	30.2
$Ce_{0.9}Pr_{0.1}O_{2-\delta}$	CeO_2	0.541	31.3
$Ce_{0.8}Pr_{0.2}O_{2-\delta}$	CeO_2	0.541	31.6
$Ce_{0.7}Pr_{0.3}O_{2-\delta}$	CeO_2	0.541	32.9
$Ce_{0.5}Pr_{0.5}O_{2-\delta}$	$CeO_2 + Pr_6O_{11}$	0.540 (CeO_2)	34.1
$Ce_{0.3}Pr_{0.7}O_{2-\delta}$	$CeO_2 + Pr_6O_{11}$	0.546 (Pr_6O_{11})	34.1
Pr_6O_{11}	Pr_6O_{11}	0.547	40.1

range from 20 to 100° with a scan rate of 0.1°/s. The mean crystallite size (D) was determined by employing peak-broadening analysis utilizing the Scherrer's equation.

3. Results and Discussion

3.1. XRD Characterization of $Ce_xPr_{1-x}O_{2-\delta}$ Mixed Oxides. Figure 1 shows the XRD patterns of $Ce_xPr_{1-x}O_{2-\delta}$ mixed oxides calcined at 500 °C. Crystalline phases were identified in comparison with two ICDD files (cubic CeO_2, PDF no. 81-0792; cubic Pr_6O_{11}, PDF no. 42-1121). Table 1 lists the lattice parameter and the mean crystallite size of cubic phase based on XRD data. It can be seen from Table 1, for $Ce_xPr_{1-x}O_{2-\delta}$ mixed oxides ($x = 0.5-0.99$), the lattice parameters are identical. This is because, when $Ce_xPr_{1-x}O_{2-\delta}$ solid solution forms, the Ce^{4+} ionic radius (0.097 nm) is very similar to that of Pr^{4+} (0.096 nm). All the $Ce_xPr_{1-x}O_{2-\delta}$ samples have similar crystallite sizes of 30−34 nm, except that $Ce_{0.99}Pr_{0.01}O_{2-\delta}$ has a size of 38.6 nm. However, the mean crystallite sizes of $Ce_xPr_{1-x}O_{2-\delta}$ mixed oxides are smaller than those of CeO_2 and Pr_6O_{11}.

3.2. Raman Characterization of $Ce_xPr_{1-x}O_{2-\delta}$ Mixed Oxides. Figure 2 shows the Laser Raman spectra of $Ce_xPr_{1-x}O_{2-\delta}$ mixed oxides excited with four excitation lasers ($\lambda = 325$ (a), 514 (b), 632.8 (c), and 785(d) nm). It can be seen that, for pure CeO_2, there is an obvious band at 465 cm^{-1} for all excitation lasers. It is ascribed to the Raman active F_{2g} mode of CeO_2, the band of a fluorite structural material. This can be viewed as a symmetric breathing mode of the oxygen atoms surrounding each cation. It also can be seen that, with increasing the Pr content, there is a small systematic shift of the bands at 465 cm^{-1} to lower frequencies, which is due to the fact that the insertion of Pr ions decreases the vibration frequency of the metal−anion band because the atomic mass of Pr is larger than that of Ce[17] and the slight change of the lattice parameter. It also indicates that the incorporation of Pr into the ceria lattices results in the formation of the solid solutions. No obvious Raman band is observed for Pr_6O_{11}. For $Ce_xPr_{1-x}O_{2-\delta}$ mixed oxides ($x = 0.10-0.99$), however, a new Raman band is observed at

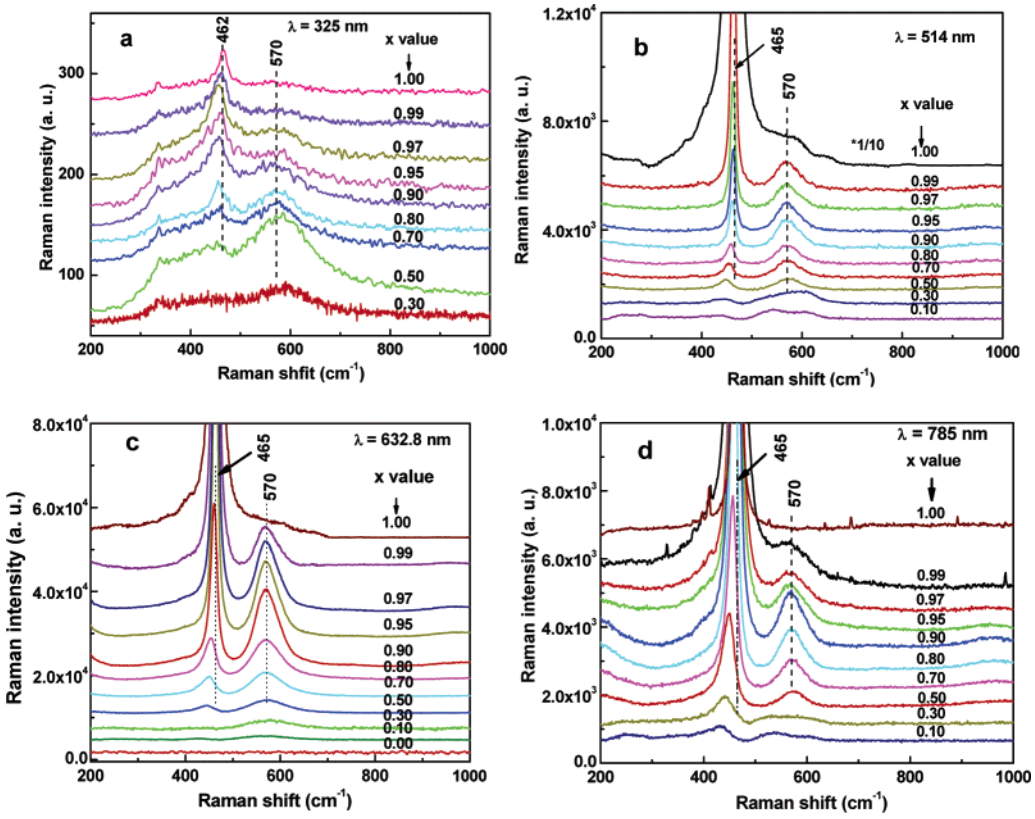

Figure 2. Laser Raman spectra with four excitation lasers for $Ce_xPr_{1-x}O_{2-\delta}$ mixed oxides ($\lambda = 325$ (a), 514 (b), 632.8 (c), and 785 (d) nm).

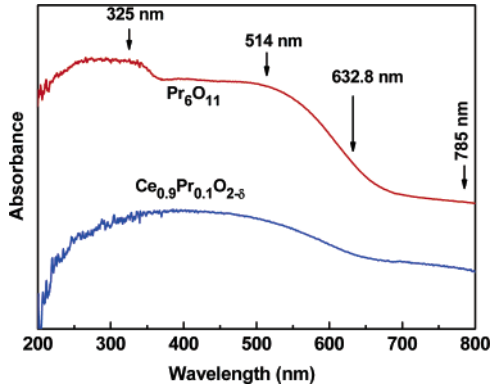

Figure 3. UV−Visible diffuse reflectance spectra of $Ce_{0.9}Pr_{0.1}O_{2-\delta}$ and Pr_6O_{11} samples.

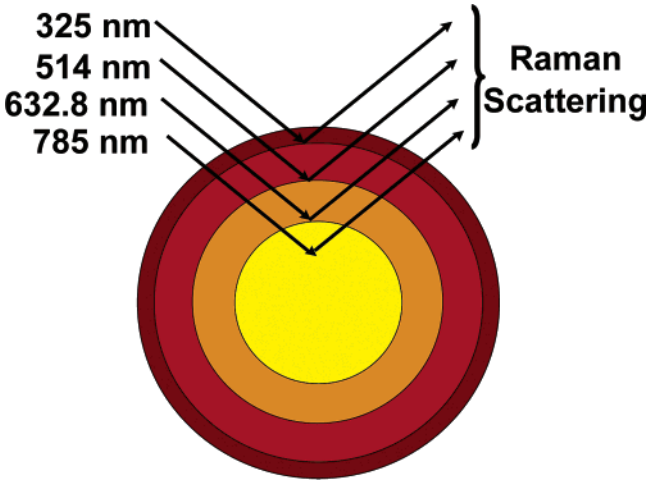

Figure 4. Schematic description obtained from laser Raman spectra with different excitation lasers and XRD.

570 cm^{-1} and its position is not influenced by the content of Pr, which is different from 465 cm^{-1}. However, the intensity of the band varies obviously with x, and a maximum is found at $x = 0.9$. McBride and co-workers[17] suggested that the band at 570 cm^{-1} can be linked to lattice defects, which results from the formation of oxygen vacancies, so that the material can absorb and give off oxygen easily and enhances OSC.[6,18] It is especially important for catalytic reactions and enhancing the activity of the oxygen ions.

3.3. The Surface and Bulk Structure of $Ce_xPr_{1-x}O_{2-\delta}$ Mixed Oxides. Figure 3 shows the UV−visible diffuse reflectance spectra of $Ce_{0.9}Pr_{0.1}O_{2-\delta}$ and Pr_6O_{11} samples. It can be seen that both samples show an absorption band from 200 to 650 nm, and the absorption intensity becomes weaker with increasing wavelength. There is almost no absorption at 785 nm. The absorption intensity of the samples follows the order: 325 nm ≈ 514 nm > 632.8 nm > 785 nm. When the sample absorbs the excitation laser strongly, it is hard to obtain Raman signals from the bulk of the samples. It was concluded that the obtained information is closer to the sample's bulk with the increase in the wavelength of the excitation laser.[15,16] A visual illustration for the different information obtained from different excitation lasers are shown in Figure 4. Among them, the Raman spectroscopy with shorter excitation laser is more surface sensitive.

Figure 5 shows the relationship of the value I_{570}/I_{465} to the Ce content under the different excitation lasers. The value I_{570}/I_{465} reflects the abundance of the oxygen vacancy caused by the replacement of Ce atom by Pr in the mixed oxide. It can be

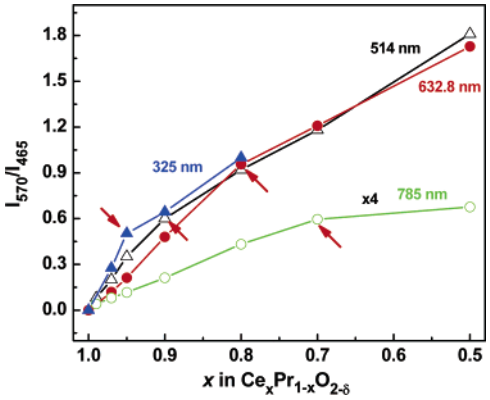

Figure 5. Relationship of the value I_{570}/I_{465} to the Ce content under four excitation lasers.

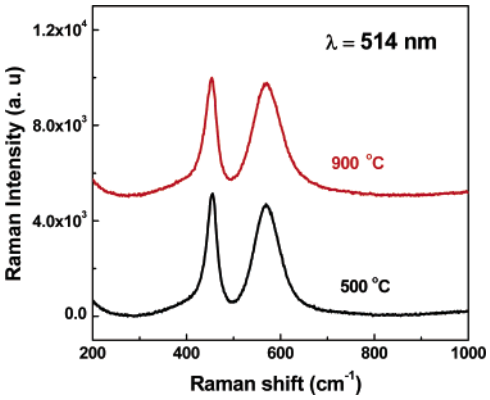

Figure 6. Laser Raman spectra of $Ce_{0.8}Pr_{0.2}O_{2-\delta}$ mixed oxide calcined at different temperatures.

seen that, for a fixed composition, the value decreases with increasing excitation laser wavelength, suggesting that there are more oxygen vacancies in the surface region of the sample. Another interesting finding is that there is an obvious inflection (pointed by arrow) in the measurement region for the relationship of the value I_{570}/I_{465} to the Ce content. The value I_{570}/I_{465} increases linearly with the decrease in the Ce content on both sides of the inflection. Besides, with the increase in the wavelength of excitation laser, the Ce content corresponding to the inflection decreases. If the distribution of Ce and Pr in the mixed oxide particles is uniform, there should not be any inflection in the relationship of the value I_{570}/I_{465} to the Ce content. Therefore, it can be considered that the composition of $Ce_xPr_{1-x}O_{2-\delta}$ mixed oxide particles in the surface region and the bulk shell might be different.

Figure 6 shows the Laser Raman spectra of $Ce_{0.8}Pr_{0.2}O_{2-\delta}$ calcined at 500 and 900 °C, respectively. Their mean crystallite sizes are 12.3 and 31.6 nm, respectively. It can be seen that the calcination temperature has no effect on the position of Raman bands and the value I_{570}/I_{465}, suggesting that they do not vary with the change of the mean crystallite size when its change range is 12.3−31.6 nm. Figure 7 shows the Laser Raman spectra of $Ce_{0.9}Pr_{0.1}O_{2-\delta}$ in different atmosphere at room temperature. It can be seen that, in air, O_2, and H_2 atmosphere, the value I_{570}/I_{465} is 0.60, 0.60, and 0.64, respectively. The higher I_{570}/I_{465} value in H_2 implies that the shortage of oxygen gas in H_2 atmosphere leads to the escape of oxygen atom in the lattice and favors the formation of oxygen vacancies. It further suggests that the band at 570 cm^{-1} is ascribed to the oxygen vacancy.

To clarify the difference between the surface and the bulk phases, the surface composition was analyzed by XPS. Table 2

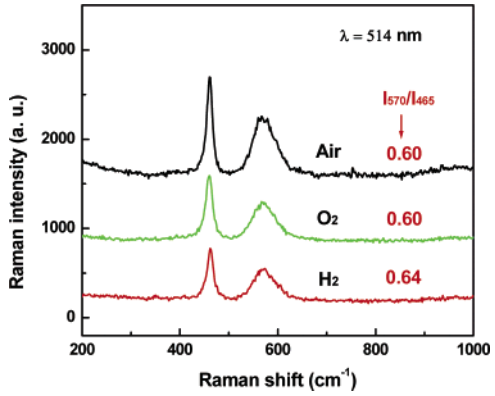

Figure 7. Laser Raman spectra of $Ce_{0.9}Pr_{0.1}O_{2-\delta}$ mixed oxide at different atmosphere.

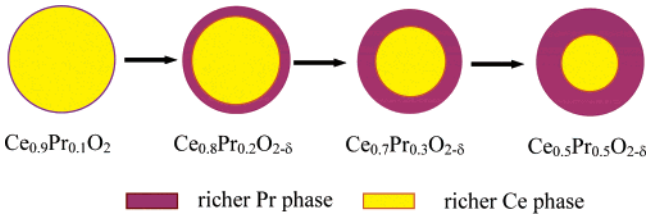

Figure 8. Schematic description of the phase change of $Ce_xPr_{1-x}O_{2-\delta}$ samples.

TABLE 2: Atomic Ratio in the Surface of the $Ce_xPr_{1-x}O_{2-\delta}$ Samples Obtained from the XPS

samples	Ce/Pr atomic ratio
$Ce_{0.8}Pr_{0.2}O_{2-\delta}$	0.65/0.35
$Ce_{0.5}Pr_{0.5}O_{2-\delta}$	0.35/0.65
$Ce_{0.3}Pr_{0.7}O_{2-\delta}$	0.15/0.85

shows the atomic ratio of Ce/Pr in the surface region of the $Ce_xPr_{1-x}O_{2-\delta}$ samples obtained from the XPS spectra. It is clear that the content of Pr in the surface region is higher than that of the nominal composition. For example, the Pr content in the surface region is 35%, while the nominal content is 20% for the $Ce_{0.8}Pr_{0.2}O_{2-\delta}$ sample. This indicates that Pr is richer in the surface region, while Ce is richer in the bulk shell. Because XPS is surface sensitive, it can be deduced that $Ce_xPr_{1-x}O_{2-\delta}$ mixed oxide is composed of rich Pr in the surface region and rich Ce in the bulk. The thickness of the surface layer with rich Pr component is related to the Ce content in the sample; when the Ce content decreases, the thickness increases. Therefore, it can be concluded that the value I_{570}/I_{465} depends on two aspects: one is the thickness and the Pr content of the surface layer and the other is the depth that the excitation laser can penetrate the sample. When one excitation laser with fixed wavelength is used, the value lies on the former. With the decrease in the Ce content of the sample, both the thickness and the Pr content of the rich Pr layer increase, therefore, the value I_{570}/I_{465} linearly increases. When the thickness of the rich Pr layer exceeds the depth that the excitation laser penetrates the sample, the value I_{570}/I_{465} only lies on the Pr content of the rich Pr layer, thus the increase in the value I_{570}/I_{465} slows down. The difference between the two speeds of the increase in the value results in the inflection. Because the depth that the excitation laser penetrates the sample varies with the wavelength of the excitation laser, the position of the inflection moves toward right with the increase in the wavelength of the excitation laser. Therefore, the change of the inflection position indicates the thickness of the rich Pr layer in the surface region varies with the Ce content. Because the mean crystallite size of $Ce_xPr_{1-x}O_{2-\delta}$ mixed oxides calcined at 900 °C is between 30 and 34 nm, it can be assumed that the cystallite size of samples are the same. A sketch that describes the dependence of the thickness of the rich Pr layer on the content of Pr is presented in Figure 8. Similar results that the composition in the surface region and the bulk shell are different were also discovered in Ce−Zr−O[6] and Ce−Cu−O[19] systems.

4. Conclusions

$Ce_xPr_{1-x}O_{2-\delta}$ mixed oxides with different composition were studied by Raman spectroscopy using four different excitation lasers and XPS analysis. It is found that the surface region and the bulk shell are different; the former is enrichment of Pr and the latter is enrichment of Ce. On the basis of the fact that the laser line with shorter wavelength is closer to the electronic adsorption of samples, it is found that the Raman information detected by short excitation laser is more sensitive to the surface region of samples. An inflection is observed in the relationship of the value I_{570}/I_{465} to the Ce content in $Ce_xPr_{1-x}O_{2-\delta}$. It is found that the position of the inflection varies with the wavelength of excitation laser, indicating that the thickness of the rich Pr layer in the surface region varies with the Ce content in $Ce_xPr_{1-x}O_{2-\delta}$ mixed oxides. The thickness of the surface layer with rich Pr increases with the decrease in the Ce content.

Acknowledgment. This work is financially supported by the Natural Science Foundation of China (grant 20473075) and the Zhejiang Provincial Nature Science Foundation of China (no. M203147).

References and Notes

(1) Zhang, J.; Ju, X.; Wu, Z. Y.; Liu, T.; Hu, T. D.; Xie, Y. N. *Chem. Mater*. **2001**, *13*, 4192.
(2) Balducci, G.; Islam, M. S.; Kašpar, J.; Fornasiero, P.; Graziani, M. *Chem. Mater*. **2000**, *12*, 677.
(3) Sayle, T.; Parkerb, C.; Sayle, D. C. *Chem. Commun*. **2004**, 2438.
(4) Wang, Z.; Feng, X. *J. Phys. Chem. B* **2003**, *107*, 13563.
(5) Shchukin, D. G.; Caruso, R. A. *Chem. Mater*. **2004**, *16*, 2287.
(6) Monte, R. D.; Kašpar, J. *J. Mater. Chem*. **2005**, *15*, 633.
(7) Laachir, A.; Perrichon, V.; Badri, A.; Lamotte, J.; Catherine, E.; Lavalley, J. C.; El Fallah, J.; Hilarie, L.; Leonormand, F.; Quemere, E.; Sauvion, G. N.; Touret, O. *J. Chem. Soc., Faraday Trans*, *1* **1991**, *87*, 1601.
(8) Kubsh, J. E.; Rieck, J. S.; Spencer, N. D. *Stud. Surf. Sci. Catal*. **1994**, *71*, 109.
(9) Sinha, A. K.; Suzuki, K. *J. Phys. Chem. B* **2005**, *109*, 1708.
(10) Luo, M. F.; Shan, W. J.; Ying, P. L.; Lu, J. Q.; Li, C. *Stud. Surf. Sci. Catal*. **2001**, *138*, 61.
(11) Yan, Z. L.; Luo, M. F.; Huang, W.; Xie, Y. L. *Chin. J. Inorg. Chem*. **2005**, *21*, 425.
(12) Stencel, J. M. *Raman Spectroscopy for Catalysis*; Van Nostrand Reinhold: New York, 1990.
(13) Campion A. In *Vibrational Spectroscopy of Molecules on Surfaces*; Yates, J. T., Jr., Madey, T. E., Eds. Plenum Press: New York, 1987; p 345.
(14) Brown, F. R.; Maskovsky, L. E. *Appl. Spectrosc*. **1977**, *31*, 44.
(15) Li, C.; Li, M. J. *J. Raman Spectrosc*. **2002**, *33*, 301.
(16) Li, M. J.; Feng, Z. C.; Ying, P. L.; Xin, Q.; Li, C. *Phys. Chem. Chem. Phys*. **2003**, *5*, 5326.
(17) Mcbride, J. R.; Hass, K. C.; Poindexter, B. D., et al. *J. Appl. Phys*. **1994**, *76*, 2435.
(18) Si, R.; Zhang, Y. W.; Li, S. J.; Lin, B. X.; Yan, C. H. *J. Phys. Chem. B* **2004**, *108*, 12481.
(19) Shan, W. J.; Feng, Z. C.; Li, Z. L.; Zhang, J.; Shen, W. J.; Li, C. *J. Catal*. **2004**, *228*, 206.